Dual Domain Motion Artifacts Correction for MR Imaging Under Guidance of K-space Uncertainty

Jiazhen Wang[1], Yizhe Yang[1], Yan Yang[1], and Jian Sun[1,2,3(✉)]

[1] Xi'an Jiaotong University, Xi'an, China
{jzwang,yyz0022}@stu.xjtu.edu.cn, {yangyan,jiansun}@xjtu.edu.cn
[2] Pazhou Laboratory (Huangpu), Guangzhou, China
[3] Peng Cheng Laboratory, Shenzhen, China

Abstract. Magnetic resonance imaging (MRI) may degrade with motion artifacts in the reconstructed MR images due to the long acquisition time. In this paper, we propose a dual domain motion correction network (D^2MC-Net) to correct the motion artifacts in 2D multi-slice MRI. Instead of explicitly estimating the motion parameters, we model the motion corruption by k-space uncertainty to guide the MRI reconstruction in an unfolded deep reconstruction network. Specifically, we model the motion correction task as a dual domain regularized model with an uncertainty-guided data consistency term. Inspired by its alternating iterative optimization algorithm, the D^2MC-Net is composed of multiple stages, and each stage consists of a k-space uncertainty module (KU-Module) and a dual domain reconstruction module (DDR-Module). The KU-Module quantifies the uncertainty of k-space corruption by motion. The DDR-Module reconstructs motion-free k-space data and MR image in both k-space and image domain, under the guidance of the k-space uncertainty. Extensive experiments on fastMRI dataset demonstrate that the proposed D^2MC-Net outperforms state-of-the-art methods under different motion trajectories and motion severities.

Keywords: Magnetic resonance imaging · Motion artifacts correction · Dual domain reconstruction · K-space uncertainty

1 Introduction

Magnetic resonance imaging (MRI) is a widely used non-invasive imaging technique. However, MRI is sensitive to subject motion due to the long time for k-space data acquisition [16]. Motion artifacts, appearing as ghosting or blurring artifacts in MR images, degrade the MR image quality [23] and affect the

J. Wang and Y. Yang—Both authors contributed equally to this work.

H. Greenspan et al. (Eds.): MICCAI 2023, LNCS 14229, pp. 293–302, 2023.
https://doi.org/10.1007/978-3-031-43999-5_28

clinical diagnosis. During the scan, it is hard for subjects to remain still, especially for pediatrics or neuro-degenerative patients. Therefore, the correction of motion artifacts in MRI has a great clinical demand.

The typical methods for motion artifacts correction in MRI include the prospective and retrospective methods. The prospective methods measure the subject motion using external tracking devices or navigators during the scan for motion correction [11]. The retrospective motion correction methods either explicitly model and correct the motion in the image reconstruction algorithm, or learn the mapping from MR image with motion artifacts to the motion-free MR image using deep learning approach. Specifically, the methods in [2,4,6,9,15] are based on a forward model of subject motion, and jointly estimate the motion parameters and MR image using the optimization algorithm. The methods in [8,12,14] introduce convolutional neural networks (CNNs) into the joint optimization procedure to learn the MR image prior. The deep learning methods in [3,10,18,19,21] directly learn the mapping from motion-corrupted MR image to motion-free MR image by designing various deep networks. Some other methods correct the motion artifacts using additional prior information, such as the different contrasts of the same object [13], self-assisted adjacent slices priors [1].

In this paper, we propose a dual domain motion correction network (i.e., D^2MC-Net) to correct the motion artifacts in 2D multi-slice MRI. Instead of explicitly estimating motion parameters, we design a dual domain regularized model with an uncertainty-guided data consistency term, which models the motion corruption by k-space uncertainty to guide the MRI reconstruction. Then the alternating iterative algorithm of the model is unfolded to be a novel deep network, i.e., D^2MC-Net. As shown in Fig. 1, the D^2MC-Net contains multiple stages, and each stage consists of two key components, i.e., k-space uncertainty module (KU-Module) and dual domain reconstruction module (DDR-Module). The KU-Module measures the uncertainty of k-space data corrupted by the motion. The DDR-Module reconstructs motion-free k-space data and MR image in both k-space and image domain under the guidance of the k-space uncertainty. Extensive experiments on fastMRI dataset demonstrate that the proposed D^2MC-Net achieves the state-of-the-art results under different motion trajectories and motion severities. For example, under severe corruption with piecewise constant motion trajectory, our result in PSNR is at least 2.11 dB higher than the existing methods, e.g., Autofocusing+ [12].

Different from the optimization-based methods [2,4,6,8,9,12,14,15], our model is based on modeling the motion corruption by k-space uncertainty without explicitly estimating the motion parameters. Different from the deep learning methods [1,3,10,18,19,21], D^2MC-Net incorporates an uncertainty-guided data consistency term into the unfolded network to guide MRI reconstruction.

2 Methods

2.1 Problem Formulation

In our approach, we model the motion corruption by measuring the uncertainty of k-space data. Specifically, we assume that the distribution of motion-corrupted k-space data $\hat{\boldsymbol{y}} \in \mathbb{C}^N$ at each position obeys a non-i.i.d. and pixel-wise Gaussian distribution, where N is the number of the k-space data. Specifically, considering the i-th position of the $\hat{\boldsymbol{y}}$, we have

$$p(\hat{y}_{[i]}|\boldsymbol{x}, \sigma_{[i]}) \sim \mathcal{N}(\hat{y}_{[i]}|(\boldsymbol{\mathcal{F}}\boldsymbol{x})_{[i]}, \sigma^2_{[i]}), \tag{1}$$

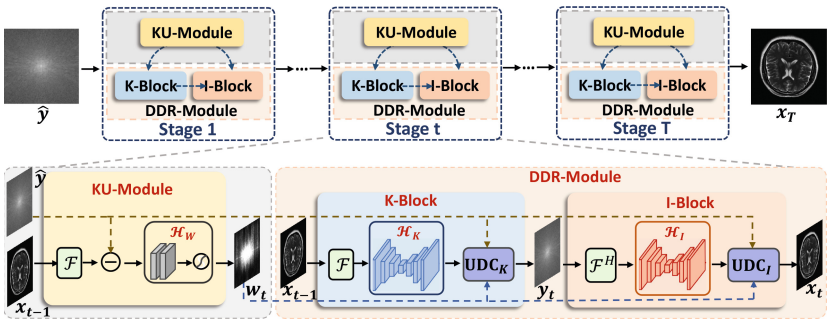

Fig. 1. The architecture of the proposed dual domain motion correction network, i.e. *D^2MC-Net*. Each stage consists of two components, i.e., k-space uncertainty module (KU-Module) and dual domain reconstruction module (DDR-Module).

where $\boldsymbol{x} \in \mathbb{C}^N$ denotes the motion-free image. $\boldsymbol{\mathcal{F}} \in \mathbb{C}^{N\times N}$ is the Fourier transform matrix. $\sigma_{[i]} \in [1, \infty)$ is the standard deviation at i-th position, which gives larger values to k-space data severely corrupted by the motion and smaller values to k-space data less affected by the motion.

Based on the above distribution model of the motion-corrupted k-space data, we propose the following maximum log-posterior estimation model:

$$\max_{\boldsymbol{x},\boldsymbol{y},\boldsymbol{w}} \log p(\boldsymbol{x}, \boldsymbol{y}, \boldsymbol{w}|\hat{\boldsymbol{y}}) = \max_{\boldsymbol{x},\boldsymbol{y},\boldsymbol{w}} \log p(\hat{\boldsymbol{y}}|\boldsymbol{x}, \boldsymbol{w}) + \log p(\boldsymbol{x}) + \log p(\boldsymbol{y}) + \text{const} \tag{2}$$

where $\boldsymbol{w} \in [0, 1]^N$ represents the k-space uncertainty with the elements $w_{[i]} = {}^1/_{\sigma_{[i]}}$. $p(\boldsymbol{x})$ and $p(\boldsymbol{y})$ are the prior distributions of the motion-free data in image domain and k-space domain. The likelihood distribution $\log p(\hat{\boldsymbol{y}}|\boldsymbol{x}, \boldsymbol{w}) = \prod_i p(\hat{y}_{[i]}|\boldsymbol{x}, \sigma_{[i]})$ has been modeled by Eq. (1). Then the solution of Eq. (2) can be converted to a dual domain regularized model with an uncertainty-guided data consistency term to correct the motion-related artifacts:

$$\begin{aligned} \boldsymbol{x}^*, \boldsymbol{y}^*, \boldsymbol{w}^* = \arg\min_{\boldsymbol{x},\boldsymbol{y},\boldsymbol{w}} & \frac{1}{2} \|\boldsymbol{w} \odot \boldsymbol{\mathcal{F}}\boldsymbol{x} - \boldsymbol{w} \odot \hat{\boldsymbol{y}}\|_2^2 + \frac{\rho}{2} \|\boldsymbol{x} - \mathcal{H}_I(\boldsymbol{x}; \theta_I)\|_2^2 \\ & + \frac{\lambda}{2} \|\boldsymbol{y} - \mathcal{H}_K(\boldsymbol{y}; \theta_K)\|_2^2 - \sum\nolimits_i^N \log w_{[i]}, \qquad s.t. \quad \boldsymbol{y} = \boldsymbol{\mathcal{F}}\boldsymbol{x} \end{aligned} \tag{3}$$

where $\mathcal{H}_I$ and $\mathcal{H}_K$ are learnable denoisers with parameters θ_I and θ_K, which adopt the U-Net [18] architecture in this paper. λ and ρ are trade-off parameters. The first term is the uncertainty-guided data consistency term corresponding to the log-likelihood $\log p(\hat{\boldsymbol{y}}|\boldsymbol{x}, \boldsymbol{w})$ which enforces consistency between the k-space data of reconstructed MR image and its motion-corrupted k-space data under the guidance of the uncertainty $\boldsymbol{w}$. The second and third terms are regularizations for imposing image-space prior $p(\boldsymbol{x})$ and k-space prior $p(\boldsymbol{y})$.

2.2 Dual Domain Motion Correction Network

Our proposed D^{2}MC-Net is designed based on the alternating optimization algorithm to solve Eq. (3). As shown in Fig. 1, taking the motion-corrupted k-space data as input, it reconstructs the motion-free MR images with T stages. Each stage consists of the k-space uncertainty module (KU-Module) and the dual domain reconstruction module (DDR-Module), respectively corresponding to the sub-problems for optimizing the k-space uncertainty $\boldsymbol{w}$, and the dual domain data including k-space data $\boldsymbol{y}$ and MR image $\boldsymbol{x}$. The KU-Module estimates the k-space uncertainty $\boldsymbol{w}$, quantifying the uncertainty of k-space data corrupted by motion. The DDR-Module is responsible for reconstructing the k-space data $\boldsymbol{y}$ and MR image $\boldsymbol{x}$, under the guidance of the k-space uncertainty $\boldsymbol{w}$. Details of these two modules at t-th stage are as follows.

K-space Uncertainty Module. This module is designed to update k-space uncertainty $\boldsymbol{w}$ in Eq. (3). If directly optimizing $\boldsymbol{w}$ in Eq. (3), $\boldsymbol{w}_t = {}^1/_{|\boldsymbol{\mathcal{F}}\boldsymbol{x}_{t-1} - \hat{\boldsymbol{y}}|}$ at t-th stage, which depends on the difference between the k-space data of reconstructed image $\boldsymbol{\mathcal{F}}\boldsymbol{x}_{t-1}$ and the motion-corrupted k-space data $\hat{\boldsymbol{y}}$. We extend this estimate to be a learnable module defined as:

$$\boldsymbol{w}_t \triangleq \mathcal{H}_W(\boldsymbol{\mathcal{F}}\boldsymbol{x}_{t-1}, \hat{\boldsymbol{y}}; \theta_W), \tag{4}$$

where $\mathcal{H}_W$ is the sub-network with parameters θ_W. When t=1, we only send $\hat{\boldsymbol{y}}$ into the KU-Module because we do not have the estimate of the reconstructed MR images in such case.

Dual Domain Reconstruction Module. This module is designed to update k-space data $\boldsymbol{y}$ and MR image $\boldsymbol{x}$ in Eq. (3) under the guidance of the uncertainty $\boldsymbol{w}$. Specifically, given the reconstructed MR image $\boldsymbol{x}_{t-1}$ from $(t-1)$-th stage and the k-space uncertainty $\boldsymbol{w}_t$, the k-space data at t-th stage is updated by:

$$\begin{aligned} \boldsymbol{y}_t &= \arg\min_{\boldsymbol{y}} \frac{1}{2} \|\boldsymbol{W}_t \boldsymbol{y} - \boldsymbol{W}_t \hat{\boldsymbol{y}}\|_2^2 + \frac{\lambda}{2} \|\boldsymbol{y} - \mathcal{H}_K(\boldsymbol{\mathcal{F}}\boldsymbol{x}_{t-1}; \theta_K)\|_2^2 \\ &= (\boldsymbol{W}_t^\top \boldsymbol{W}_t + \lambda \boldsymbol{I})^{-1} (\boldsymbol{W}_t^\top \boldsymbol{W}_t \hat{\boldsymbol{y}} + \lambda \mathcal{H}_K(\boldsymbol{\mathcal{F}}\boldsymbol{x}_{t-1}; \theta_K)) \\ &\triangleq \mathrm{UDC}_K \circ \mathcal{H}_K(\boldsymbol{\mathcal{F}}\boldsymbol{x}_{t-1}; \theta_K), \end{aligned} \tag{5}$$

where $\boldsymbol{W}_t = \mathrm{diag}(\boldsymbol{w}_t) \in [0, 1]^{N \times N}$ is a diagonal matrix, thus the matrix inversion in Eq. (5) can be computed efficiently. Equation (5) is defined as k-space reconstruction block (K-Block), solving the sub-problem for optimizing k-space

data $\boldsymbol{y}$ in Eq. (3). Equation (5) can be implemented by firstly computing $\mathcal{H}_K$, followed by the k-space uncertainty-guided data consistency operator UDC_K in Eq. (5). Similarly, given the updated uncertainty $\boldsymbol{w}_t$ and k-space data $\boldsymbol{y}_t$, the MR image at t-th stage is updated by:

$$\begin{aligned}\boldsymbol{x}_t &= \arg\min_{\boldsymbol{x}} \frac{1}{2}\|\boldsymbol{W}_t\boldsymbol{\mathcal{F}}\boldsymbol{x} - \boldsymbol{W}_t\hat{\boldsymbol{y}}\|_2^2 + \frac{\rho}{2}\|\boldsymbol{x} - \mathcal{H}_I(\boldsymbol{\mathcal{F}}^H\boldsymbol{y}_t;\theta_I)\|_2^2 \\ &= \boldsymbol{\mathcal{F}}^H(\boldsymbol{W}_t^\top\boldsymbol{W}_t + \rho\boldsymbol{I})^{-1}(\boldsymbol{W}_t^\top\boldsymbol{W}_t\hat{\boldsymbol{y}} + \rho\boldsymbol{\mathcal{F}}\mathcal{H}_I(\boldsymbol{\mathcal{F}}^H\boldsymbol{y}_t;\theta_I)) \\ &\triangleq \text{UDC}_I \circ \mathcal{H}_I(\boldsymbol{\mathcal{F}}^H\boldsymbol{y}_t;\theta_I).\end{aligned} \tag{6}$$

Equation (6) is defined as image reconstruction block (I-Block), solving the sub-problem for optimizing MR image $\boldsymbol{x}$ in Eq. (3). Equation (6) can be implemented by firstly computing $\mathcal{H}_I$, followed by the image domian uncertainty-guided data consistency operator UDC_I in Eq. (6). The K-Block and I-Block are combined as the dual domain reconstruction module (DDR-Module) to sequentially reconstruct the k-space data $\boldsymbol{y}_t$ and MR image $\boldsymbol{x}_t$ at t-th stage.

In summary, by connecting the k-space uncertainty module and dual domain reconstruction module alternately, we construct a multi-stage deep network (i.e., D^{2}MC-Net) for motion artifacts correction as shown in Fig. 1.

2.3 Network Details and Training Loss

In the proposed D^{2}MC-Net, we use $T = 3$ stages for speed and accuracy trade-off. Each stage has three sub-networks (i.e., $\mathcal{H}_W$, $\mathcal{H}_K$ and $\mathcal{H}_I$) as shown in Fig. 1. $\mathcal{H}_K$ and $\mathcal{H}_I$ adopt U-Net [18] architecture which contains five encoder blocks and four decoder blocks followed by a 1×1 convolution layer for the final output. Each block consists of two 3×3 convolution layers, an instance normalization (IN) layer and a ReLU activation function. The average pooling and bilinear interpolation layers are respectively to reduce and increase the resolution of the feature maps. The number of output feature channels of the encoder and decoder blocks in U-Net are successively 32, 64, 128, 256, 512, 256 128, 64, 32. The structure of $\mathcal{H}_W$ is Conv→IN→ReLU→Conv→Sigmoid, where Conv denotes a 3×3 convolution layer. The number of output feature channels for these two convolution layers are 64 and 2, respectively.

The overall loss function in image space and k-space is defined as:

$$\mathcal{L} = \sum\nolimits_{t=1}^{T} \gamma\|\boldsymbol{y}_t - \boldsymbol{y}_{gt}\|_1 + \|\boldsymbol{x}_t - \boldsymbol{x}_{gt}\|_1 + (1 - \text{SSIM}(\boldsymbol{x}_t, \boldsymbol{x}_{gt})), \tag{7}$$

where $\boldsymbol{x}_t$ and $\boldsymbol{y}_t$ are the reconstructed MR image and k-space data at t-th stage. $\boldsymbol{x}_{gt}$ and $\boldsymbol{y}_{gt}$ are the motion-free MR image and k-space data. SSIM [22] is the structural similarity loss. γ is a hyperparameter to balance the different losses in dual domain, and we set $\gamma = 0.001$. The Adam optimizer with mini-batch size of 4 is used to optimize the network parameters. The initial value of the learning rate is 1×10^{-4} and divided by 10 at 40-th epoch. We implement the proposed D^{2}MC-Net using PyTorch on one Nvidia Tesla V100 GPU for 50 epochs.

3 Experiments

Dataset. We evaluate our method on the T2-weighted brain images from the fastMRI dataset [7], and we randomly select 78 subjects for training and 39 subjects for testing. The in-plane matrix size of the subjects is resized to 384 × 384, and the number of slices varies from the subjects. Sensitivity maps are estimated using the ESPIRiT algorithm [20] for coil combination.

Motion Artifacts Simulation. We simulate in-plane and through-plane motion according to the forward model $\hat{y} = M\mathcal{F}T_\theta x$ [2], where $T_\theta \in \mathbb{R}^{N\times N}$ is the rigid-body motion matrix parameterized by a vector of translations and rotations $\theta \in \mathbb{R}^3 \times [-\pi, \pi]^3$. $M \in \{0, 1\}^{N\times N}$ is the diagonal mask matrix in k-space. And we keep 7% of the k-space lines in the center for preventing excessive distortion of the images. The motion vectors are randomly selected from a Gaussian distribution $\mathcal{N}(0, 10)$. We follow the motion trajectories (i.e., piecewise constant, piecewise transient and Gaussian) used in the paper [5] to simulate motion. In addition, to generate various motion severities, each motion level has a series of motion-corrupted k-space lines: 0–30%, 0–50%, and 0–70% of the total of k-space lines for mild, moderate, and severe, respectively. Finally, the motion-corrupted volume k-space data is cut into slice data and sent to the proposed D^{2}MC-Net.

Table 1. Quantitative comparison of different methods on fastMRI under different motion trajectories and motion severities, in PSNR (dB), SSIM and NRMSE.

Motion Trajectories	Methods	Mild			Moderate			Severe		
		PSNR	SSIM	NRMSE	PSNR	SSIM	NRMSE	PSNR	SSIM	NRMSE
Piecewise Constant	Corrupted	33.76	0.9081	0.1344	30.71	0.8563	0.1895	28.52	0.8134	0.2366
	U-Net	35.84	0.9571	0.1023	32.65	0.9345	0.1494	32.14	0.9168	0.1527
	UPGAN	36.06	0.9537	0.0986	34.01	0.9287	0.1246	32.19	0.8781	0.1530
	SU-Net	35.92	0.9541	0.1012	34.00	0.9378	0.1254	32.97	0.9241	0.1389
	Alternating	37.08	0.9538	0.0879	34.51	0.9305	0.1186	32.33	0.9064	0.1506
	Autofocusing+	37.43	0.9559	0.0847	35.57	0.9356	0.1044	33.17	0.9115	0.1360
	Ours	**41.00**	**0.9761**	**0.0567**	**37.79**	**0.9594**	**0.0806**	**35.28**	**0.9399**	**0.1066**
Piecewise Transient	Corrupted	32.78	0.8317	0.1407	30.04	0.7750	0.1934	28.56	0.7469	0.2301
	U-Net	35.58	0.9511	0.1053	33.67	0.9338	0.1310	32.49	0.9217	0.1494
	UPGAN	37.57	0.9526	0.0809	35.50	0.9339	0.1026	34.20	0.9220	0.1191
	SU-Net	37.50	0.9540	0.0815	35.28	0.9363	0.1052	34.56	0.9335	0.1269
	Alternating	37.09	0.9447	0.0854	35.15	0.9264	0.1068	34.02	0.9170	0.1217
	Autofocusing+	37.21	0.9415	0.0850	35.58	0.9271	0.1021	34.37	0.9138	0.1169
	Ours	**38.94**	**0.9607**	**0.0691**	**37.37**	**0.9493**	**0.0828**	**35.96**	**0.9380**	**0.0973**
Gaussian	Corrupted	32.71	0.8293	0.1419	30.12	0.7749	0.1915	28.67	0.7444	0.2270
	U-Net	34.78	0.9484	0.1174	33.83	0.9357	0.1299	34.05	0.9268	0.1222
	UPGAN	36.25	0.9477	0.0938	35.94	0.9363	0.0974	34.42	0.9208	0.1160
	SU-Net	37.06	0.9523	0.0864	34.92	0.9402	0.1100	34.49	0.9290	0.1169
	Alternating	37.02	0.9432	0.0861	34.72	0.9194	0.1121	34.43	0.9196	0.1160
	Autofocusing+	37.75	0.9425	0.0792	35.50	0.9275	0.1033	34.67	0.9153	0.1129
	Ours	**39.40**	**0.9615**	**0.0654**	**37.58**	**0.9502**	**0.0807**	**36.21**	**0.9396**	**0.0945**

Performance Evaluation. We compare the proposed D^{2}MC-Net with four deep learning methods (i.e., U-Net [18], UPGAN [21], SU-Net [1], and Alternating [17]), and an optimization-based method (i.e., Autofocusing+ [12]). The motion-corrupted image without motion correction is denoted as "Corrupted". In Table 1, we show the quantitative results of different methods under different motion trajectories and motion severities. Compared with "Corrupted", these deep learning methods improve the reconstruction performance. By explicitly estimating motion parameters, Autofocusing+ produces better results than deep learning methods. Our method achieves the best results in all experiments, mainly because the uncertainty-guided data consistency term is introduced into the unfolded deep network to guide MRI reconstruction. The qualitative comparison results under the severe corruption with piecewise constant motion trajectory are shown in Fig. 2. In comparison, our method has the smallest reconstruction error and recovers finer image details while suppressing undesired artifacts. The PSNR and SSIM values in Fig. 2 also demonstrate the superiority of our method. For example, the PSNR value of our method is 3.06 dB higher than that of SU-Net [1].

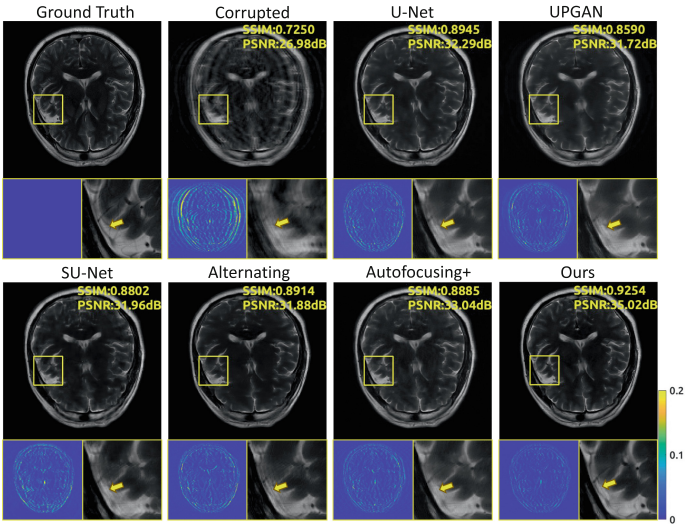

Fig. 2. Qualitative results of different methods under severe corruption with the piecewise constant motion trajectory.

Table 2. Ablation study of the key components of D^{2}MC-Net.

Methods	KU-Module	K-Block	I-Block	PSNR	SSIM	NRMSE
Baseline			✓	34.53	0.9416	0.1172
w/o K-Block	✓		✓	36.17	0.9503	0.0968
Ours ($\boldsymbol{w} = \mathbf{0}$)		✓	✓	35.18	0.9438	0.1089
Ours ($\boldsymbol{w} = \mathbf{1}$)		✓	✓	36.84	0.9521	0.0880
Ours	✓	✓	✓	**37.79**	**0.9594**	**0.0806**

Effectiveness of the Key Components. We evaluate the effectiveness of these key components, including KU-Module, K-Block, and I-Block in Fig. 1, under the moderate corruption with piecewise constant motion trajectory. In Table 2, (A) "Baseline" denotes the reconstruction model $x_t = \mathcal{H}_I(\boldsymbol{x}_{t-1}; \theta_I)), t = 1 \cdots T$. (B) "$w/o$ K-Blcok" denotes our D^{2}MC-Net without K-Blocks. (C) "Ours ($\boldsymbol{w} = \mathbf{0}$)" denotes our D^{2}MC-Net without KU-Modules, and the k-space uncertainty $\boldsymbol{w} = \mathbf{0}$. (D) "Ours ($\boldsymbol{w} = \mathbf{1}$)" denotes our D^{2}MC-Net without KU-Modules and the k-space uncertainty $\boldsymbol{w} = \mathbf{1}$. (E) "Ours" is our full D^{2}MC-Net equipped with KU-Modules, K-Blocks and I-Blocks. As shown in Table 2, our results are better than all the compared variants, showing the effectiveness of the k-space uncertainty and dual-domain reconstruction. Compared with methods that do not use motion-corrupted k-space data (i.e., "Ours ($\boldsymbol{w} = \mathbf{0}$)") and fully use motion-corrupted k-space data (i.e., "Ours ($\boldsymbol{w} = \mathbf{1}$)") in reconstruction, our method selectively uses the motion-corrupted k-space data under the guidance of the learned k-space uncertainty $\boldsymbol{w}$, and achieves higher performance.

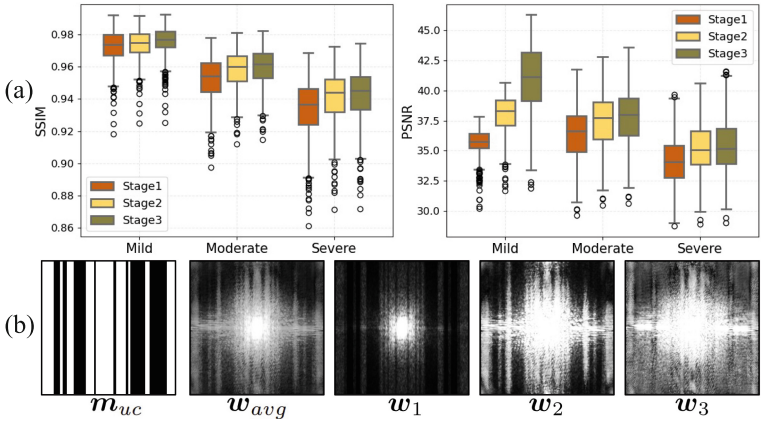

Fig. 3. (a) Qualitative results from different stages of the D^{2}MC-Net under different severities with the piecewise constant motion trajectory. (b) The visual results of $\boldsymbol{w}$ from different stages under moderate piecewise constant motion.

Table 3. Ablation study of the hyperparameters in the loss function.

Hyperparameters	$\gamma = 1$	$\gamma = 0.1$	$\gamma = 0.01$	$\gamma = 0.001$	$\gamma = 0.0001$	$\gamma = 0$
PSNR	37.19 dB	37.20 dB	37.41 dB	**37.79 dB**	37.44 dB	37.10 dB

Effect of Number of Stages. We evaluate the effect of the number of stage T in D^{2}MC-Net. Figure 3(a) reports the results of different T under different motion severities with piecewise constant motion trajectory. We observe that increasing the number of stages in D^{2}MC-Net achieves improvement in PSNR and SSIM metrics, but costs more memory and computational resources.

Visualization of the Uncertainty $\boldsymbol{w}$. The estimated k-space uncertainties of all stages are visualized in Fig. 3(b). As we can see, the averaged k-space uncertainty $\boldsymbol{w}_{avg}$ over all stages approximates the real motion trajectory mask $\boldsymbol{m}_{uc}$ with ones indicating the un-corrupted k-space lines.

Effect of Different Loss Functions. We also investigate the effect of the k-space loss by adjusting the values of hyperparameters γ in Eq. (7). The PSNR results under the piecewise constant moderate motion are shown in Table 3. From these results, our method achieves the best performance at $\gamma = 0.001$.

4 Conclusion

In this paper, we proposed a novel dual domain motion correction network (D^2MC-Net) to correct the motion artifacts in MRI. The D^2MC-Net consists of KU-Modules and DDR-Modules. KU-Module measures the uncertainty of k-space data corrupted by motion. DDR-Module reconstructs the motion-free MR images in k-space and image domains under the guidance of the uncertainty estimated by KU-Module. Experiments on fastMRI dataset show the superiority of the proposed D^2MC-Net. In the future work, we will extend the D^2MC-Net to be a 3D motion correction method for 3D motion artifacts removal.

Acknowledgements. This work is supported by National Key R&D Program of China (2022YFA1004201), National Natural Science Foundation of China (12090021, 12125104, 61721002, U20B2075).

References

1. Al-masni, M.A., et al.: Stacked u-nets with self-assisted priors towards robust correction of rigid motion artifact in brain mri. Neuroimage **259**, 119411 (2022)
2. Alexander, L., Hannes, N., Pohmannand, R., Bernhard, S.: Blind retrospective motion correction of MR images. Magn. Reson. Med. **70**(6), 1608–1618 (2013)
3. Armanious, K., et al.: MedGAN: medical image translation using GANs. Comput. Med. Imaging Graph. **79**, 101684 (2020)
4. Atkinson, D., Hill, D.L.G., Stoyle, P.N.R., Summers, P.E., Keevil, S.F.: Automatic correction of motion artifacts in magnetic resonance images using an entropy focus criterion. IEEE Trans. Med. Imaging **16**(6), 903–910 (1997)
5. Ben, A.D., et al.: Retrospective motion artifact correction of structural MRI images using deep learning improves the quality of cortical surface reconstructions. Neuroimage **230**, 117756 (2021)
6. Daniel, P., et al.: Scout accelerated motion estimation and reduction (SAMER). Magn. Reson. Med. **87**(1), 163–178 (2022)
7. Florian, K., et al.: fastMRI: a publicly available raw k-space and DICOM dataset of knee images for accelerated MR image reconstruction using machine learning. Radiol. Artif. Intell. **2**(1) (2020)
8. Haskell, M.W., et al.: Network accelerated motion estimation and reduction (NAMER): convolutional neural network guided retrospective motion correction using a separable motion model. Magn. Reson. Med. **82**(4), 1452–1461 (2019)

9. Haskell, M.W., Cauley, S.F., Wald, L.L.: Targeted motion estimation and reduction (TAMER): data consistency based motion mitigation for MRI using a reduced model joint optimization. IEEE Trans. Med. Imaging **37**(5), 1253–1265 (2018)
10. Junchi, L., Mehmet, K., Mark, S., Jie, D.: Motion artifacts reduction in brain MRI by means of a deep residual network with densely connected multi-resolution blocks (DRN-DCMB). Magn. Reson. Imaging **71**, 69–79 (2020)
11. Kay, N., Peter, B.: Prospective correction of affine motion for arbitrary MR sequences on a clinical scanner. Magn. Reson. Med. **54**(5), 1130–1138 (2005)
12. Kuzmina, E., Razumov, A., Rogov, O.Y., Adalsteinsson, E., White, J., Dylov, D.V.: Autofocusing+: Noise-resilient motion correction in magnetic resonance imaging. In: Wang, L., Dou, Q., Fletcher, P.T., Speidel, S., Li, S. (eds.) MICCAI 2022. LNCS, vol. 13436, pp. 365–375. Springer, Cham (2022). https://doi.org/10.1007/978-3-031-16446-0_35
13. Lee, J., Kim, B., Park, H.: MC2-Net: motion correction network for multi-contrast brain MRI. Magn. Reson. Med. **86**(2), 1077–1092 (2021)
14. Levac, B., Jalal, A., Tamir, J.I.: Accelerated motion correction for MRI using score-based generative models. arXiv (2022). https://arxiv.org/abs/2211.00199
15. Lucilio, C.G., Teixeira, R.P.A.G., Hughes, E.J., Hutter, J., Price, A.N., Hajnal, J.V.: Sensitivity encoding for aligned multishot magnetic resonance reconstruction. IEEE Trans. Comput. Imaging **2**(3), 266–280 (2016)
16. Maxim, Z., Julian, M., Michael, H.: Motion artifacts in MRI: a complex problem with many partial solutions. J. Magn. Reson. Imaging **42**(4), 887–901 (2015)
17. Singh, N.M., Iglesias, J.E., Adalsteinsson, E., Dalca, A.V., Golland, P.: Joint frequency and image space learning for MRI reconstruction and analysis. J. Mach. Learn. Biomed. Imaging (2022)
18. Ronneberger, O., Fischer, P., Brox, T.: U-Net: convolutional networks for biomedical image segmentation. In: Navab, N., Hornegger, J., Wells, W.M., Frangi, A.F. (eds.) MICCAI 2015. LNCS, vol. 9351, pp. 234–241. Springer, Cham (2015). https://doi.org/10.1007/978-3-319-24574-4_28
19. Thomas, K., Karim, A., Jiahuan, Y., Bin, Y., Fritz, S., Sergios, G.: Retrospective correction of motion-affected MR images using deep learning frameworks. Magn. Reson. Med. **82**(4), 1527–1540 (2019)
20. Uecker, M., et al.: ESPIRiT-an eigenvalue approach to autocalibrating parallel MRI: where sense meets grappa. Magn. Reson. Med. **71**(3), 990–1001 (2014)
21. Upadhyay, U., Chen, Y., Hepp, T., Gatidis, S., Akata, Z.: Uncertainty-guided progressive GANs for medical image translation. In: de Bruijne, M., et al. (eds.) MICCAI 2021. LNCS, vol. 12903, pp. 614–624. Springer, Cham (2021). https://doi.org/10.1007/978-3-030-87199-4_58
22. Wang, Z., Bovik, A.C., Sheikh, H.R., Simoncelli, E.P.: Image quality assessment: from error visibility to structural similarity. IEEE Trans. Image Process. **13**(4), 600–612 (2004)
23. Wood, M.L., Henkelman, R.M.: MR image artifacts from periodic motion. Med. Phys. **12**(2), 143–151 (1985)